Biases in the calculation of Southern Hemisphere mean baroclinic eddy growth rate

Ian Simmonds[1] and Eun-Pa Lim[2]

Received 13 October 2008; revised 13 November 2008; accepted 2 December 2008; published 13 January 2009.

[1] The maximum Eady growth rate measure of baroclinic instability is very commonly used in the literature. Its average is usually calculated directly from the time-mean flow. It is suggested here that this approach is not entirely suitable, but rather one should obtain the Eady growth rates at all relevant synoptic times and average these. It is found at the 850 hPa level in the Southern Hemisphere that the time-mean of the instantaneous rates exceed those calculated from the time-mean field over much of the mid and high latitudes, and the difference is even more marked at 500 hPa. At both levels the axes of the maxima Eady growth rates are displaced to the south. Some implications are discussed, including the need for caution when diagnosing changes in cyclone properties from changes in Eady growth rate calculated directly from the time-mean flow in climate change model simulations. **Citation:** Simmonds, I., and E.-P. Lim (2009), Biases in the calculation of Southern Hemisphere mean baroclinic eddy growth rate, *Geophys. Res. Lett.*, *36*, L01707, doi:10.1029/2008GL036320.

1. Introduction

[2] In their elegant survey of baroclinic instability theory *Pierrehumbert and Swanson* [1995] commented that 'baroclinic instability is unambiguously successful in explaining why differentially heated rotating planets spontaneously generate transient eddies... and has yielded insights as to the interplay of baroclinic eddies and static stability...' (p. 461). One focus of the present work is to explore an aspect of that interplay and the consequences of the temporal variations of meridional temperature gradients (or vertical shear) and static stability. There are many facets to the interaction of these two quantities which give rise to, at first sight, surprising results, and it is clear that the understanding of the influence of Southern Hemisphere (SH) static stability on a range of timescales is essential for obtaining a more comprehensive picture of cyclonic development in a broad range of contexts. For example, *Walland and Simmonds* [1999] discussed how the southern Semiannual Oscillation (and its associated cyclonic features) exhibits two high latitude surface pressure minima during the year, with the one occurring in October being more intense than that in March. The associated meridional temperature gradient at these latitudes is, however, stronger in March. They found this apparent paradox to be explained when allowance was made for the seasonal evolution of static stability, and then the larger peak of baroclinicity occurred in October. In general, the complexity of the high southern latitude environment dictates that nonlinearities and covariances (on synoptic timescales, for example) between fundamental variables are strong [e.g., *Simmonds and Dix*, 1989; *Gulev*, 1997; *Simmonds et al.*, 2005], meaning that the estimation of nonlinear quantities (e.g., surface fluxes) from mean fields (in either a temporal sense (e.g., monthly or seasonal) or spatial sense (e.g., zonal average)) is liable to significant error.

[3] Most studies of the instabilities of the SH circulation have been undertaken with the time mean basic flows. Among these are those conducted with normal mode analysis [e.g., *Berbery and Vera*, 1996; *Walsh et al.*, 2000], and those with sophisticated global instability models [e.g., *Frederiksen and Frederiksen*, 2007]. An issue of relevance to these is that, given the intimate connection between the mean flow and cyclonic activity, it is not entirely clear how the "basic state" should be defined in such studies. *Trenberth*'s [1981] analysis of SH eddies led him to comment that 'the "basic state" for instability studies is not necessarily the same as the observed mean flow' (p. 2604). *Holloway* [1986] also remarked that '... there is the disturbingly nontrivial problem of distinguishing mean and fluctuating fields... This problem is compounded when we ask the dynamical question, how are mean and fluctuating fields interrelated?' (pp. 91–92). Similar sentiments were recently voiced by *Descamps et al.* [2007].

[4] Here we address an aspect of this issue by considering the sensitivity of mean baroclinic growth rates calculated from the *Eady* [1949] formulation. Under this very commonly-used framework the maximum growth rate of eddies is proportional to the ratio of the meridional temperature gradient and the Brunt-Väisälä frequency. Because this expression for the growth rates is nonlinear, it is clear that a true appreciation of the mean Eady growth rate cannot strictly be determined from the mean atmospheric state, but rather the mean rate should be determined from the mean of the instantaneous growth rates calculated over some extended period. (Only a handful of (Northern Hemisphere (NH)) studies have adopted this approach, but they presented no quantification of the sensitivity of the growth rate calculated in these two ways.) Our goal in this paper is to quantify and explain the bias in calculating Eady growth rates using a time-mean state.

2. Data and Methods

2.1. Meteorological Analysis Set

[5] Our investigation is conducted with the Japanese 25-year reanalysis (JRA-25) [*Onogi et al.*, 2007]. This set

[1]School of Earth Sciences, University of Melbourne, Melbourne, Victoria, Australia.
[2]Centre for Australian Weather and Climate Research, Bureau of Meteorology, Melbourne, Victoria, Australia.

0094-8276/09/2008GL036320

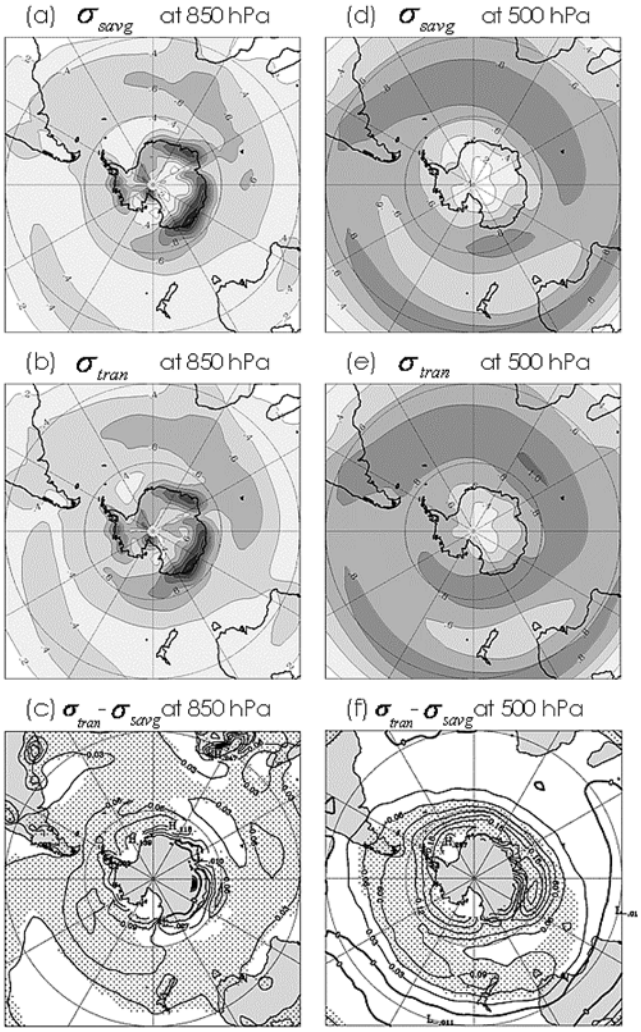

Figure 1. Climatology of the maximum Eady growth rate calculated with (a and d) seasonal mean vertical shear and N and (b and e) 6 hourly vertical shear and N, and (c and f) the difference (left) at 850 hPa and (right) at 500 hPa in JJA. The contour interval is 0.2 day^{-1} in Figures 1a, 1b, 1d, and 1e and 0.03 day^{-1} in Figures 1c and 1f. The stippled area in Figures 1c and 1f indicates that the difference between Figures 1a and 1b and between Figures 1d and 1e is statistically significant at the 95% confidence level. The data poleward of 75°S are masked in Figures 1c and 1f.

was explicitly chosen for our analysis because it may have some advantages over sets previously used for eddy growth studies. For example, the time series of global precipitation is superior to that in ERA-40 [*Uppala et al.*, 2005]. (The moisture analysis scheme used in ERA-40 resulted in very large global average differences between precipitation and evaporation (about 0.6 mm day^{-1}), whereas the JRA-25 reanalyses are much closer to balance (particularly since 1995) [*Uppala et al.*, 2008].) These and other features mean that the important source of latent heat, especially in the tropics, is well simulated in the JRA-25 assimilating model and this, in turn, would be expected to have global consequences for the quality of the reanalysis. Forcing in the tropical regions has a very strong impact on the baroclinic zones in the high southern latitudes [e.g., *Simmonds and Jacka*, 1995; *Lim and Simmonds*, 2008] and on teleconnections [*Karoly et al.*, 1989]. The precise treatment of tropical latent heat release significantly impacts on extratropical weather and climate.

[6] The JRA-25 assimilation model has a resolution of T106L40. The reanalysis data set is archived every 6 hours and available on a global 2.5° × 2.5° latitude-longitude grid. The parts of the JRA-25 to be used here cover the period of 1979–2007.

2.2. Eady Growth Rate

[7] Our analysis of baroclinic growth follows the maximum growth rates for the configuration of the Eady problem. The Eady growth rate is given by

$$\sigma_E = 0.3098 \frac{|f| \left| \frac{\partial U(z)}{\partial z} \right|}{N} \quad (1)$$

[*Vallis*, 2006] where N is the Brunt-Väisälä frequency (where $N^2 = \frac{g}{\theta}\frac{\partial \theta}{\partial z}$, g being the acceleration due to gravity, z the vertical coordinate, and θ the potential temperature) and f is the Coriolis parameter. $U(z)$ is the vertical profile of the eastward wind component.

[8] We perform our examination for Winter (June–August (JJA)) and Summer (December–February (DJF)), and σ_E is calculated at 500 and 850 hPa. Our investigations have been performed at these lower- and mid-troposphere levels as they present different insights, and it is not clear as to the most informative level(s) over which to assess baroclinic characteristics [see, e.g., *Hoskins and Valdes*, 1990; *Lim and Simmonds*, 2007]. *Hoskins and Valdes* [1990] calculated their parameter 'over a depth of 2 km just above the boundary layer', and presented the results of their (NH) calculations at about 780 hPa. Our perspective is that over the SH with its relatively modest topography over the regions of interest a slightly lower level is appropriate and we have performed our analysis at 850 hPa. To calculate the maximum growth rates at the 500 hPa level the potential temperatures at 300, 500 and 700 hPa are used to estimate the Brunt-Väisälä frequency and the vertical shear. (The vertical shear in equation (1) was expressed in terms of the meridional temperature gradient using the thermal wind equation, and use was also made of the hydrostatic equation.) Similarly, the growth rates at 850 hPa were determined from temperatures at 700, 850 and 1000 hPa.

[9] We first calculated the seasonal average fields and followed the usual method of using these to estimate the mean Eady growth rate using equation (1). Then we computed the climatology of the Eady growth rate for each season (σ_{savg}). In a second approach we calculated the instantaneous σ_E from each of the 6 hourly data, and calculated the long term averages of these growth rates (σ_{tran}). For ease of reference below, we will refer to these techniques for computing σ_{savg} and σ_{tran} as methods M (for mean) and T (for transients), respectively.

3. Results

3.1. Mean Winter and Summer Growth Rates

[10] We firstly show the 850 hPa σ_E calculated from the JRA-25 winter mean fields (Figure 1a). Consistent with

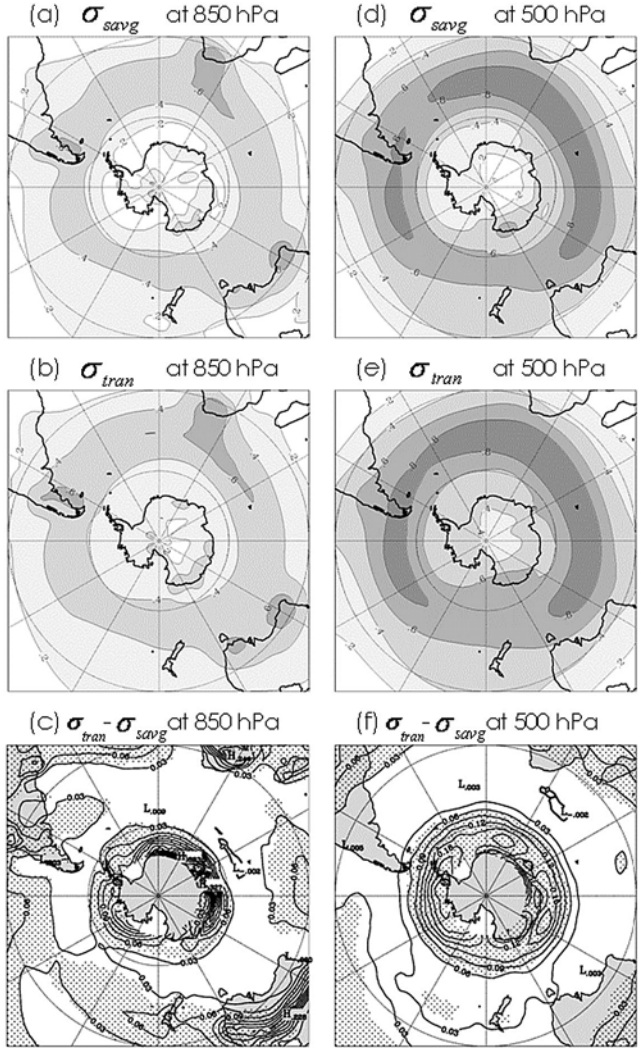

Figure 2. Climatology of the maximum Eady growth rate calculated with (a and d) seasonal mean vertical shear and N and (b and e) 6 hourly vertical shear and N, and (c and f) the difference (left) at 850 hPa and (right) at 500 hPa in DJF The contour interval is 0.2 day^{-1} in Figures 2a, 2b, 2d, and 2e and 0.03 day^{-1} in Figures 2c and 2f. The stippled area in Figures 2c and 2f indicates that the difference between Figures 2a and 2b and between Figures 2d and 2e is statistically significant at the 95% confidence level. The data poleward of 75°S are masked in Figures 2c and 2f.

other studies [e.g., *Berbery and Vera*, 1996, Figure 1b] there is a broad region to the east of South America over which the growth rates exceed 0.4 day^{-1}. Further east this ribbon spirals in toward the Antarctic continent and it lies to the south of 60°S in the region just upstream of the Drake Passage. Embedded in this ribbon is a region in the east Atlantic and western Indian Oceans over which the growth rate exceeds 0.6 day^{-1}. Another belt of high growth rate is found in the subtropical Pacific. The largest rates are found around the entire coast of East Antarctica.

[11] When we determine the σ_E from the average of the rates calculated every 6 hours (method T), we get a similar pattern (Figure 1b), but a number of important differences are apparent. It is clear that the growth rates are enhanced in the midlatitudes and especially off the coast of much of West Antarctica. To make these differences more obvious we have plotted in Figure 1c the difference between the two calculations (σ_{tran} minus σ_{savg}). It can be seen that the differences exceed 0.03 day^{-1} (or an increase in the apparent growth rate of about 10%) over most of the extratropics. Differences in excess of 0.06 day^{-1} are seen off West Antarctica.

[12] Similar displays for the 500 hPa level are presented in Figures 1d–1f. Here the Eady growth rates assume similar structure to that at 850 hPa but have a more ordered and large-scale organization. The split jet structure in Australian and west Pacific longitudes is very apparent in the results using the two methods (Figures 1d and 1e), but overall it is clear that larger growth rates are calculated with method T. The difference map (Figure 1f) shows that in the midlatitudes the significant changes are confined to the Pacific sector (particularly in the lee of Tasmania and New Zealand). Method T results in increasingly greater growth rates with latitude which culminate in differences in excess of 0.15 day^{-1} off much of Antarctica. Reference back to Figures 1d and 1e shows how these represent large changes to the diagnosed baroclinicity around and to the south of 60°S, and are consistent with the high observed rates of cyclogenesis at these high latitudes [*Turner et al.*, 1998; *Simmonds and Keay*, 2000; *Simmonds et al.*, 2003]. The structure of the difference plot indicates that σ_{tran} has the zones of maximum baroclinicity shifted to the south. We finally note that the structure of the difference maps at 850 and 500 hPa are rather different, although both show the greatest changes around the Antarctic continent.

[13] Turning now to the summer case, the 850 hPa maximum Eady growth rates for this season calculated with methods M and T are shown in Figures 2a and 2b. As is known the structure is more zonally symmetric than in winter, and the summer rates exceed those of winter over the south of Australia and the subpolar region in the Pacific Ocean. The difference map (Figure 2c) reveals that σ_{tran} has higher growth rates over virtually the entire hemisphere with differences which are significant over all the regions south of 60°S, and in the Pacific and Indian Ocean subtropics. Of particular note are the large increases over the hot southern African and Australian continents.

[14] Similar plots for the eddy growth rates at 500 hPa are displayed in Figures 2d–2f. As for the winter case the overall structure of σ_E is dominated by the largest scales. An enhancement of the rates and a southward shift of their maxima when method T is used are clear from Figures 2d and 2e. Both σ_{tran} and σ_{savg} have their axes of maximum growth at about 50°S, particularly in the Indian and eastern Atlantic Oceans. The difference map (Figure 2f) reveals similarities to that in winter (Figure 1f), although the changes obtained when using method T off the Antarctic coast are larger in summer, and particularly so in the high variability regions of the Amundsen, Bellingshausen and Weddell Seas [*Jones and Simmonds*, 1993]. In contrast to the winter case the significant differences are confined to the region south of 55°S. We finally note that the significant increases in summer 850 hPa σ_{tran} over Australia and southern Africa are also apparent (to a more modest extent) at 500 hPa.

3.2. Reasons for the Bias in Mean Growth Rates

[15] Over virtually all regions of the plots we have shown the mean maximum Eady growth rate calculated from the mean of the 6 hourly growth rates (σ_{tran}) exceeds those calculated directly from the seasonal mean states (σ_{savg}). One of the reasons for this is that the time mean of the absolute values of the shear in equation (1) will never be less than the absolute value of the shear of the mean eastward wind. However, even if the shear was always positive (i.e., eastward wind increasing with height), there are other factors which dictate that the two methods of calculating the mean Eady growth rate will differ. This can easily be shown if we decompose the expression in equation (1). Letting S denote the modulus of the shear, σ_E is proportional to $S(1/N)$. By performing the standard (temporal) decomposition we can write

$$\overline{S\frac{1}{N}} = \overline{S}\,\overline{\left(\frac{1}{N}\right)} + \overline{S'\left(\frac{1}{N}\right)'} \tag{2}$$

where the overbar represents the time-mean and the prime the deviations from that mean. One can write

$$\overline{\left(\frac{1}{N}\right)} = \frac{1}{\overline{N}} + D$$

If all values of N are positive (as is virtually always true for the reanalysis) and at least two are different, it follows from basic arithmetic theory that D is positive (i.e., the mean of the reciprocals is greater than the reciprocal of the mean). Inserting this expression into equation (2) we obtain

$$\overline{S\frac{1}{N}} = \overline{S}\frac{1}{\overline{N}} + \overline{S}D + \overline{S'\left(\frac{1}{N}\right)'} \tag{3}$$

The term on the LHS of equation (3) is that calculated by method T, while the first term on the RHS represents the growth rate calculated by the traditional method (i.e., method M). The two differ due to the second and third terms on the RHS of equation (3), the former being always positive and the latter representing the temporal covariance of the shear and the buoyancy period.

4. Discussion and Conclusions

[16] Our investigation has been conducted with the Eady growth rate, a very commonly used diagnostic of baroclinic instability. Even though some of the assumptions made in deriving the Eady expression for the growth rate are not entirely justified (e.g., it is assumed that cyclones retain their radius during development [e.g., *Simmonds*, 2000; *Rudeva and Gulev*, 2007], and that a number of influences including horizontal shears [*Barcilon and Blumen*, 1995], moist processes [*Frierson*, 2008] and sphericity are neglected), it yields neat and tractable solutions which are easily understood and are clearly of immense value. One of the rationales for writing this paper was that the calculation of mean Eady growth rates (from the time-mean fields) is ubiquitous in the literature, and it is of importance to highlight some of the biases which are inherent in this method by which the mean rate is calculated.

[17] In summary, we have shown that the SH mean maximum Eady growth rate shows considerable sensitivity to the method by which it is calculated. Because the expression for σ_E is nonlinear, its mean calculated from the time-mean state will differ from that calculated from the averages of the Eady growth rate calculated at a number of synoptic times. We have argued that it is the latter calculation which is more appropriate. Significant bias occurs in the 'traditional' method of calculating the growth rate because of nonlinearities and covariances. These factors mean that the mean Eady growth rates are overwhelmingly greater when calculated from the synoptic data. In addition, the axes of the maxima of σ_E are displaced to the south when this method is used. In closing, we remark that our analysis has implications for the interpretation of changes in cyclogenesis under global warming (and, indeed, reinforces the importance of retaining an event-based perspective on the maintenance of climate and its change [e.g., *Koch et al.*, 2006; *Simmonds et al.*, 2008]). Studies (for the NH) have indicated that simulated changes in cyclone behavior are 'broadly consistent' with changes in the Eady growth rates calculated from the changed basic *mean* state [e.g., *Teng et al.*, 2008]. However, as we have seen, there are many subtle interactions between variations in vertical shear and static stability, especially in the SH [e.g., *Lim and Simmonds*, 2008]. Our results indicate that considerable caution should be exercised in interpreting changes in cyclone properties from changes in Eady growth rate calculated directly from the time-mean flow. A similar message emerges from the idealized model investigations of *Frierson* [2008].

[18] **Acknowledgments.** We are grateful to JMA-CRIEPI for providing the reanalysis data in the public domain and to Kevin Keay for help in data extraction. Parts of this work were made possible by grants from the Australian Research Council and from the Antarctic Science Advisory Committee.

References

Barcilon, A., and W. Blumen (1995), The Eady problem with linear horizontal shear, *Dyn. Atmos. Oceans*, *22*, 115–133.

Berbery, E. H., and C. S. Vera (1996), Characteristics of the Southern Hemisphere winter storm track with filtered and unfiltered data, *J. Atmos. Sci.*, *53*, 468–481.

Descamps, L., D. Ricard, A. Joly, and P. Arbogast (2007), Is a real cyclogenesis case explained by generalized linear baroclinic instability?, *J. Atmos. Sci.*, *64*, 4287–4308.

Eady, E. T. (1949), Long waves and cyclone waves, *Tellus*, *1*, 33–52.

Frederiksen, J. S., and C. S. Frederiksen (2007), Interdecadal changes in Southern Hemisphere winter storm track modes, *Tellus, Ser. A*, *59*, 599–617, doi:10.1111/j.1600-0870.2007.00264x.

Frierson, D. M. W. (2008), Midlatitude static stability in simple and comprehensive general circulation models, *J. Atmos. Sci.*, *65*, 1049–1062.

Gulev, S. K. (1997), Climatologically significant effects of space-time averaging in the North Atlantic sea-air heat flux fields, *J. Clim.*, *10*, 2743–2763.

Holloway, G. (1986), Eddies, waves, circulation, and mixing: Statistical geofluid mechanics, *Annu. Rev. Fluid Mech.*, *18*, 91–147.

Hoskins, B. J., and P. J. Valdes (1990), On the existence of storm-tracks, *J. Atmos. Sci.*, *47*, 1854–1864.

Jones, D. A., and I. Simmonds (1993), Time and space spectral analyses of Southern Hemisphere sea level pressure variability, *Mon. Weather Rev.*, *121*, 661–672.

Karoly, D. J., R. A. Plumb, and M. Ting (1989), Examples of the horizontal propagation of quasi-stationary waves, *J. Atmos. Sci.*, *46*, 2802–2811.

Koch, P., H. Wernli, and H. C. Davies (2006), An event-based jet-stream climatology and typology, *Int. J. Climatol.*, *26*, 283–301.

Lim, E.-P., and I. Simmonds (2007), Southern Hemisphere winter extratropical cyclone characteristics and vertical organization observed with the ERA-40 reanalysis data in 1979–2001, *J. Clim.*, *20*, 2675–2690.

Lim, E.-P., and I. Simmonds (2008), Effect of tropospheric temperature change on the zonal mean circulation and SH winter extratropical cyclones, *Clim. Dyn.*, doi:10.1007/s00382-008-0444-0.

Onogi, K., et al. (2007), The JRA-25 reanalysis, *J. Meteorol. Soc. Jpn.*, *85*, 369–432.

Pierrehumbert, R. T., and K. L. Swanson (1995), Baroclinic instability, *Annu. Rev. Fluid Mech.*, *27*, 419–467.

Rudeva, I., and S. K. Gulev (2007), Climatology of cyclone size characteristics and their changes during the cyclone life cycle, *Mon. Weather Rev.*, *135*, 2568–2587.

Simmonds, I. (2000), Size changes over the life of sea level cyclones in the NCEP reanalysis, *Mon. Weather Rev.*, *128*, 4118–4125.

Simmonds, I., and M. Dix (1989), The use of mean atmospheric parameters in the calculation of modeled mean surface heat fluxes over the world's oceans, *J. Phys. Oceanogr.*, *19*, 205–215.

Simmonds, I., and T. H. Jacka (1995), Relationships between the interannual variability of Antarctic sea ice and the Southern Oscillation, *J. Clim.*, *8*, 637–647.

Simmonds, I., and K. Keay (2000), Mean Southern Hemisphere extratropical cyclone behavior in the 40-year NCEP-NCAR reanalysis, *J. Clim.*, *13*, 873–885.

Simmonds, I., K. Keay, and E.-P. Lim (2003), Synoptic activity in the seas around Antarctica, *Mon. Weather Rev.*, *131*, 272–288.

Simmonds, I., A. Rafter, T. Cowan, A. B. Watkins, and K. Keay (2005), Large-scale vertical momentum, kinetic energy and moisture fluxes in the Antarctic sea-ice region, *Boundary Layer Meteorol.*, *117*, 149–177.

Simmonds, I., C. Burke, and K. Keay (2008), Arctic climate change as manifest in cyclone behavior, *J. Clim.*, *21*, 5777–5796.

Teng, H., W. M. Washington, and G. A. Meehl (2008), Interannual variations and future change of wintertime extratropical cyclone activity over North America in CCSM3, *Clim. Dyn.*, *30*, 673–686.

Trenberth, K. E. (1981), Observed Southern Hemisphere eddy statistics at 500mb: Frequency and spatial dependence, *J. Atmos. Sci.*, *38*, 2585–2605.

Turner, J., G. J. Marshall, and T. A. Lachlan-Cope (1998), Analysis of synoptic-scale low pressure systems within the Antarctic Peninsula sector of the circumpolar trough, *Int. J. Climatol.*, *18*, 253–280.

Uppala, S. M., et al. (2005), The ERA-40 re-analysis, *Q. J. R. Meteorol. Soc.*, *131*, 2961–3012.

Uppala, S., D. Dee, S. Kobayashi, P. Berrisford, and A. Simmons (2008), Towards a climate data assimilation system: Status update of ERA-Interim, *ECMWF Newsl.*, *115*, 12–18. (Available at http://www.ecmwf.int/publications/newsletters/pdf/115.pdf)

Vallis, G.K. (2006), *Atmospheric and Oceanic Dynamics: Fundamentals and Large-Scale Circulation*, Cambridge Univ. Press, New York.

Walland, D., and I. Simmonds (1999), Baroclinicity, meridional temperature gradients, and the southern Semiannual Oscillation, *J. Clim.*, *12*, 3376–3382.

Walsh, K. J. E., I. Simmonds, and M. Collier (2000), Sigma-coordinate calculation of topographically forced baroclinicity around Antarctica, *Dyn. Atmos. Oceans*, *33*, 1–29.

E.-P. Lim, Centre for Australian Weather and Climate Research, Bureau of Meteorology, GPO Box 1289K, Melbourne, Vic 3001, Australia.

I. Simmonds, School of Earth Sciences, University of Melbourne, Melbourne, Vic 3010, Australia. (simmonds@unimelb.edu.au)